Chinese Chemical Letters 34 (2023) 108055

Contents lists available at ScienceDirect

Chinese Chemical Letters

journal homepage: www.elsevier.com/locate/cclet

Structures and magnetic relaxation properties of cyclopentadienyl/β-diketonate/trispyrazolylborate hybridized dysprosium single-molecule magnets

Lu Zhang[a,1], Jin Xiong[b,1], Yin-Shan Meng[a,*], Tao Liu[a,*]

[a] State Key Laboratory of Fine Chemicals, Dalian University of Technology, Dalian 116024, China
[b] Department of Chemistry, Carnegie Mellon University, Pittsburgh, PA 15213, United States

ARTICLE INFO

Article history:
Received 27 October 2022
Revised 16 November 2022
Accepted 9 December 2022
Available online 10 December 2022

Keywords:
Single-molecule magnets
Lanthanide complexes
Magnetic anisotropy
Magnetic relaxations
Quantum tunneling of magnetization

ABSTRACT

The combination of cyclopentadiene, β-diketonate and tripyrazoylborate ligands with dysprosium ion afforded five mononuclear compounds: $[(Cp)_2Dy(Tp^*)]$ (**1Dy**), $[(Cp)Dy(Tp^*)Cl(THF)]$ (**2Dy**), [(Cp)Dy(Tp)Cl(THF)] (**3Dy**), [(DBM)Dy(Tp)Cl(THF)] (**4Dy**), $[\{(Tp)Dy(DBM)_2(H_2O)\}\cdot THF]$ (**5Dy**) (Cp = cyclopentadiene; Tp^* = hydrotris(3,5-dimethyl-1-pyrazolyl)borate; Tp = hydrotris(1-pyrazolyl)borate; DBM = dibenzoylmethanoate). Magnetic study revealed that **1Dy** and **3Dy** exhibited typical butterfly-type hysteresis. AC susceptibility study combined with *ab initio* calculations indicated that the magnetic relaxation behaviors of **1Dy**–**4Dy** were governed by the Orbach and Raman processes under applied DC field. Moreover, **3Dy** showed two-step magnetic relaxation, which was attributed to the static disordering of the coordinated THF molecule. Magnetic anisotropy analysis indicated that it was the relative strength of the interactions between Dy^{III} and surrounding ligands that determined the orientation of the magnetic easy axis.

© 2023 Published by Elsevier B.V. on behalf of Chinese Chemical Society and Institute of Materia Medica, Chinese Academy of Medical Sciences.

Single-molecule magnet (SMM) is a type of magnetic bistable material that can exhibit magnetic hysteresis and slow magnetic relaxation below the blocking temperature [1–5]. In the recent decades, there has been growing research interests and efforts in this area, because SMM provides an ideal platform for investigating the critical properties that connect the classical and quantum world, in addition to its potential applications in high-density information storage, quantum computing, spintronic devices, *etc.* [6–9]. The lanthanide-based compounds are widely exploited, because the trivalent lanthanide ions, especially the non-Kramers Tb^{III}, Kramers Dy^{III} and Er^{III} ions feature strong spin-orbit coupling, large ground spin state and magnetic anisotropy. Since the early reports on double-decker phthalocyanide-based $[Pc_2Tb]^-$ [10], a number of mononuclear SMMs have been synthesized [11–14]. The multidentate ligands such as porphyrins [15,16], polyoxometalates [17,18], cyclomultienes [19,20], β-diketonates [21–23], tripyrazoylborates [24,25] and Schiff bases [22,26,27], have been widely applied to construct SMMs. Breakthroughs have also been achieved recently. For example, the symmetry-controlled pseudo-D_{5h} Dy-SIMs represented the first example of SMM whose energy barrier surpasses 1000 K [28]; the very recent isolated dysprosium metallocene exhibited the blocking temperature beyond the liquid nitrogen temperature and ignited the passion for searching more excellent SMMs [29]. Generally, the thermally activated spin reversal goes through the following processes: (1) The one-phonon Direct process between the *quasi*-degenerate ground state for the non-Kramers systems; (2) The two-phonon Orbach process that goes through the first excited state; (3) The Raman process that involves the virtual excited state. The reported SMMs especially the SIMs featuring high energy barriers usually involve more than one magnetic relaxation processes [30]. The quantum tunneling and Raman process sometimes play an important role in the low temperature region, suggesting that the effective energy barrier is not the sole parameter to be optimized to achieve the high-performance SMMs. Both the static electronic structure and the spin-phonon coupling may play crucial roles in determining the magnetic relaxation properties, wherein the spin-phonon coupling can be largely affected by the surrounding ligands with different rigidity [31–33]. With this in mind, we aim to investigate the influences of cyclopentadienes, β-diketonates and trispyrazolylborates on their magnetic relaxation properties. Despite these ligands have been widely used in constructing lanthanide-based SMMs, the comparison study of them has not been exploited. Herein, we report the synthesis, structural charac-

* Corresponding authors.
E-mail addresses: mengys@dlut.edu.cn (Y.-S. Meng), liutao@dlut.edu.cn (T. Liu).
[1] These authors contribute equally to this work.

https://doi.org/10.1016/j.cclet.2022.108055
1001-8417/© 2023 Published by Elsevier B.V. on behalf of Chinese Chemical Society and Institute of Materia Medica, Chinese Academy of Medical Sciences.

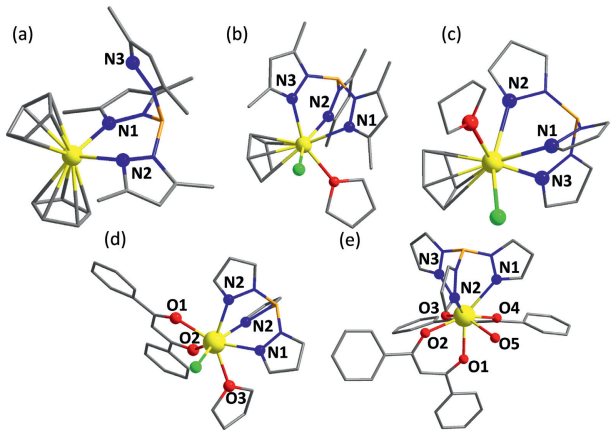

Fig. 1. (a–e) Crystal structures of **1Dy–5Dy** . Color code: Dy, yellow; C, grey; N, blue; O, red; Cl, green; B, orange. H atoms were omitted for clarity.

terizations, magnetic investigations of five dysprosium compounds: $[(Cp)_2Dy(Tp^*)]$ (**1Dy**) (Cp = cyclopentadiene; Tp^* = hydrotris(3,5-dimethyl-1-pyrazolyl)borate), $[(Cp)Dy(Tp^*)Cl(THF)]$ (**2Dy**), [(Cp)Dy(Tp)Cl(THF)] (**3Dy**) (Tp = hydrotris(1-pyrazolyl)borate; DBM = dibenzoylmethanoate), [(DBM)Dy(Tp)Cl(THF)] (**4Dy**), $[\{(Tp)Dy(DBM)_2(H_2O)\}\cdot THF]$ (**5Dy**). *Ab initio* calculations were carried out to exploit the detailed electronic structures and magnetic anisotropies of these complexes.

Complexes **1Dy**–**4Dy** are air- and moisture-sensitive and should be stored in an inert atmosphere. Complex **5Dy** can be obtained in the presence of water, whose lattice solvent molecule THF is easy to lose when exposed to the air. It is interesting that the reaction of $[Cp_2DyCl]_x$ and KTp^* shows different reactivity in toluene and THF, resulting in complex **1Dy** and **2Dy**, respectively. From **1Dy** to **5Dy**, the coordinating anions can be systematically changed from Cp^- and Tp^{*-} to Tp^- and DBM^-, providing a platform to investigate their influences on the magnetic properties. Details of crystallographic data and refinement information were provided in Tables S1 and S2, Figs. S1–S5 (Supporting information).

For **1Dy**, the Dy^{III} ion is capped by the two Cp^- anions (Fig. 1a). The Dy–C bond lengths are in the range of 2.59(1)–2.68(1) Å. Near the equatorial plane, the Tp^- anion connects the central Dy^{III} ion with two nitrogen atoms, leaving one pyrazolyl ring uncoordinated. The Dy–N1 and Dy–N2 distances are 2.421(7) and 2.409(6) Å, respectively. The Dy–N bond lengths are slightly longer than that of the reported $[(Cp^*)_2Dy(Tp)]$. The bending angle of Cnt–Dy–Cnt (Cnt = centroid of Cp ring) is 127.2(2)°.

When the raw product of **1Dy** $[(Cp_2)Dy(Tp^*)]$ was recrystallized in THF, one of the Cp^- anions was protonated and dissociated, forming the complex **2Dy** $[(Cp)Dy(Tp^*)Cl(THF)]$. The Dy^{III} ion is coordinated by one Cp^- anion, one Tp^{*-} anion, one chloride ion and one neutral THF (Fig. 1b). The Dy–C bond lengths are in the range of 2.684(5)–2.728(4) Å, which are slightly longer than that of **1Dy**. All of the three pyrazolyl rings are coordinated to the Dy^{III} ion, giving the Dy–N bond lengths of 2.433(3)–2.527(3) Å. The neighboring molecules form the weak $\pi\cdots\pi$ interactions (3.524 Å) between the adjacent pyrazolyl rings (Fig. S2). The Dy–Cl and Dy–O bond lengths are 2.614(1) and 2.407(2) Å, respectively. The local coordination sphere of Dy^{III} ion can be treated as a distorted octahedron, wherein the dihedral angle between the plane consisting of three N atoms and the plane consisting of Cl, O and centroid of Cp^- is 8.4(1)°.

The Tp^{*-} anion in **2Dy** can be replaced by the Tp^- anion, resulting in a structurally similar complex **3Dy** (Fig. 1c). **3Dy** shows smaller Dy–C bond lengths (2.643(3)–2.689(3) Å) than that of **2Dy**, possibly due to the less steric hindrance. The Dy–N bond lengths are in the range of 2.439(2)–2.469(2) Å. It is worth mentioning that

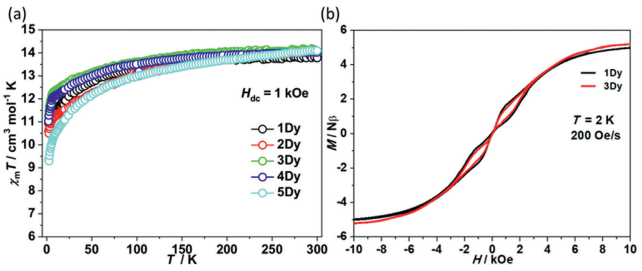

Fig. 2. (a) $\chi_m T$ *vs.* T plots for **1Dy**–**5Dy** under a 1 kOe DC field. (b) Hysteresis for **1Dy** and **3Dy** at 2 K . The field-sweeping rate was 200 Oe/s.

the coordinated THF molecule shows the static disordering, which may affect the dynamic relaxation of magnetization behavior. The dihedral angle between the plane consisting of three N atoms and the plane consisting of Cl, O and the centroid of Cp^- ion is 15°.

Complex **4Dy** [(DBM)Dy(Tp)Cl(THF)] and **5Dy** $[\{(Tp)Dy(DBM)_2(H_2O)\}\cdot THF]$ were synthesized by reacting the precursor $[TpDyCl_2(THF)_{1.5}]$ with corresponding equivalents of deprotonated DBM ligand. X-ray diffraction analysis revealed that there are seven coordinating atoms in the coordinating sphere of **4Dy** (Fig. 1d). The central Dy^{III} ion is capped by the tridentate Tp^- anion with the Dy–N bond lengths of 2.463(3)–2.482(2) Å. The Dy–O(DBM) bond lengths of 2.255(2)–2.268(2) Å are much smaller than the neutral water coordinated one (Dy–O(H_2O): 2.391(7) Å) because of the stronger electron-donating character of the DBM^- ligand. For **5Dy**, there are two DBM^- anions chelating the Dy^{III} ion, the Dy–N distances (2.514(6)-2.542(5) Å) become longer, indicating that the DBM^- anions generate greater electron repulsion with the 4f electrons (Fig. 1e). The stronger electron donor DBM^- will also have an impact on its magnetic anisotropy.

Direct current susceptibility data were collected from 2 K to 300 K under a 1 kOe DC field (Fig. 2a). At ambient temperature, the $\chi_m T$ values for **1Dy**–**5Dy** are 13.78, 14.03, 14.08, 13.94 and 14.09 cm^3 K/mol, respectively, in good agreement with the theoretical value for the free Dy^{III} ion (14.17 cm^3 K/mol, $^6H_{15/2}$, $S = 5/2$, $J = 15/2$ and $g = 4/3$) [34]. Upon cooling, all complexes undergo a gradual decrease of $\chi_m T$ values in the measured temperature range, which is indicative of the typical depopulation of Stark sublevels. The $\chi_m T$ values then reach the minimum of 10.95, 10.60, 11.22, 11.03 and 9.35 cm^3 K/mol at 2 K, respectively. The lower $\chi_m T$ value of **5Dy** suggests that the ground doublet is highly mixed with smaller $|M_J|$ components. The field-dependent magnetization behaviors were recorded from 0 to 50 kOe at selected temperatures. As shown in Fig. S6 (Supporting information), the magnetization values of **2Dy**, **4Dy** and **5Dy** are around 5 Nβ, far from the saturated value for the free Dy^{III} ion. The magnetization *versus* H/T plots all show the non-superposition character, indicating the significant magnetic anisotropy of Dy^{III} ion. It is worth noting that **1Dy** and **3Dy** can exhibit butterfly-type hysteresis under a field-sweeping rate of 200 Oe/s (Fig. 2b), which is indicative of single-molecule magnets. By contrast, no hysteresis was observed in **2Dy**, **4Dy** and **5Dy**.

Alternative current susceptibility study as the function of temperature and frequency were performed on this series of complexes (Figs. S7 and S8 in Supporting information). For **1Dy**, a clear frequency-dependent behavior in both in-phase and out-of-phase signals were observed in the absence of DC field (Fig. S7a). Below 10 K, the position of resonant peaks remained unchanged at around 3000 Hz, which corresponds to the temperature-independent quantum tunneling of magnetization (QTM). Above 10 K, the relaxation of magnetization was thermally activated, thus the position of resonant peaks exhibited temperature dependence. The in-phase and out-of-phase susceptibilities were plotted as Ar-

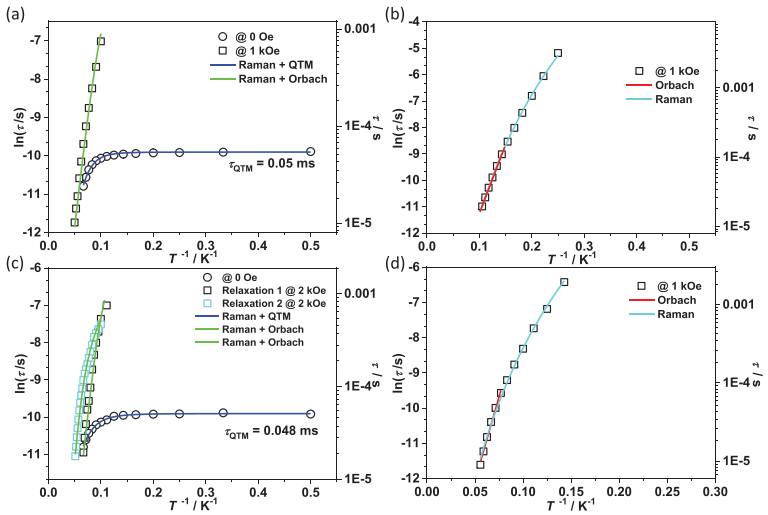

Fig. 3. (a–d) $\ln\tau$ *vs.* T^{-1} plots for **1Dy**–**4Dy**. The blue lines represent the combined Raman and QTM fitting using the equation $1/\tau = B \times T^{n} + 1/\tau_{QTM}$. The turquoise lines represent the Raman fitting using the equation $1/\tau = B \times T^{n}$. The green lines represent the combined Raman and Orbach fitting using the equation $1/\tau = C \times T^{n} + 1/\tau_{0} \times \exp(-U_{eff}/T)$. The red lines represent the Orbach fitting using $1/\tau = 1/\tau_{0} \times \exp(-U_{eff}/T)$.

gand diagram and fitted by the generalized Debye model [35]. The extracted relaxation time for the QTM process is 0.05 ms below 10 K (Fig. 3a and Fig. S9 in Supporting information). Above 10 K, the $\ln(\tau)$ *versus* T^{-1} plots showed an obvious curvation, suggesting that the Arrhenius-type Orbach process may not be involved. Then the combination of Raman process and QTM process was accounted for interpreting the plot [36]. The fitting parameters n was 5.27, C was 0.0177 s^{-1} K^{-n} and τ_{QTM} was 0.05 ms. Since the external field can remove the degeneracy of the ground doublet and suppress the QTM, an optimized field of 1 kOe was applied. As shown in Fig. 3a, the thermally activated relaxation was observed in the measured temperature range, indicating that the QTM was sufficiently quenched. However, the plots of relaxation times as the function of inverse temperature still showed the non-linearity. Therefore, the fitting with the Orbach process and Raman process was applied, yielding the effective energy barrier U_{eff} of 123 K, pre-exponential factor τ_0 of 1.72×10^{-8} s, n of 4.77 and C of 0.0638 s^{-1} K^{-n}. It is noteworthy that only using the Raman term cannot well reproduce the $\ln(\tau)$ *versus* T^{-1} plots.

For **2Dy**, the AC susceptibility study also revealed the typical frequency-dependent behavior in the absence of a DC field (Fig. S7b). Unfortunately, the relaxation times cannot be extracted, because the magnetic relaxation rate is beyond the detecting limitation of our equipment. Such fast relaxation is caused by the QTM within the ground doublet. When a 1.5 kOe DC field was applied, the temperature-dependent relaxation appeared between 2 K and 10 K (Fig. S8b). The resonant peak corresponding to 10000 Hz is at 9.5 K, much lower than that of **1Dy** (19 K). The fitted energy barrier by applying the Arrhenius law in the higher temperature region is 53 K with the τ_0 of 6.89×10^{-8} s (Fig. 3b and Fig. S10 in Supporting information). The $n(\tau)$ *versus* T^{-1} plots can also be well fitted by the power law, resulting in the n of 6.65 and C of 0.0193 s^{-1} K^{-n}. This suggests that the thermal magnetic relaxation may also originate from the Raman process.

3Dy showed a more complicated magnetic relaxation behavior (Figs. S7c and S8c). In the absence of a DC field, **3Dy** showed the quantum tunneling of magnetization with the τ_{QTM} of 0.048 ms, similar to that of **1Dy** (Fig. 3c). The power law fitting for the $\ln(\tau)$ *versus* T^{-1} plots gave the n value of 4.36 and C value of 0.204 s^{-1} K^{-n}, where the QTM relaxation time was fixed at 0.048 ms. When a 2 kOe DC field was applied, the QTM relaxation was quenched and the out-of-phase susceptibilities showed broad resonant peaks in the temperature range from 6 K to 11 K, suggesting the occurrence of a two-step thermally activated relaxation. At 14 K, the fast relaxation process (R1) disappeared. The relaxation times were extracted from the temperature-dependent out-of-phase signals (Fig. S11 in Supporting information), resulting in two distinct $\ln(\tau)$ *versus* T^{-1} curves. For the fast relaxation process (R1), the $\ln(\tau)$ *versus* T^{-1} plots can be well fitted by utilizing the Raman and Orbach terms. The fitted energy barrier is 136 K, which is comparable to that of **1Dy**. However, the n value (3.87) for **3Dy** is much smaller than the expected value (9) for Kramers ions. For the slow relaxation process (R2), the $\ln(\tau)$ *versus* T^{-1} plots exhibit the linearity at high temperature region. The fitted energy barrier is 168 K, which is 32 K higher than that of R1 process. At lower temperatures, the relaxation is dominated by the Raman process with a small n value of 3.42. Such a two-step relaxation behavior is not uncommon and has been reported in several lanthanide SMMs. The multi-step relaxation behaviors are usually caused by the different paramagnetic ions with different coordination spheres or by the different relaxation pathways through different excited states. For **3Dy**, the fitted energy barriers of R1 and R2 processes are numerically close to each other. According to the calculated energy levels of the low-lying states (see vide infra), the energy separation between the first and second excited states is much larger than 32 K. By careful checking the crystal structure, we find that the coordinated THF molecule shows two static conformations. The difference in the THF conformations acts as a small perturbation on the crystal field splitting of the central Dy^{III} ion and leads to two relaxation processes. This multi-step relaxation behavior has also been observed in lanthanide metallocene SMMs [37] and β-diketonate-supported dysprosium SMMs [38], for which the different conformations of the coordinated ligands are the main reason for the multi-step relaxations.

The further dynamic magnetic study indicated that **4Dy** exhibited very fast magnetic relaxation behavior even under 1 kOe DC field (Figs. S7d and S8d). The fitted energy barrier is 95 K with τ_0 of 4.85×10^{-8} s. Besides, the temperature-dependent relaxation times can also be fitted by the power law ($\tau^{-1} = C \times T^{n}$; $n = 0.0173$, $C = 5.36$), suggesting that the second order Raman process may play a part (Fig. 3d and Fig. S12 in Supporting information). For **5Dy**, no frequency- or temperature-dependent AC susceptibilities can be observed under any applied DC fields (Fig. S7e), indicating that **5Dy** is not a single-molecule magnet.

The magnetic study demonstrated that replacing the cyclopentadienyl ligand with trispyrazolylborate or β-diketonate signifi-

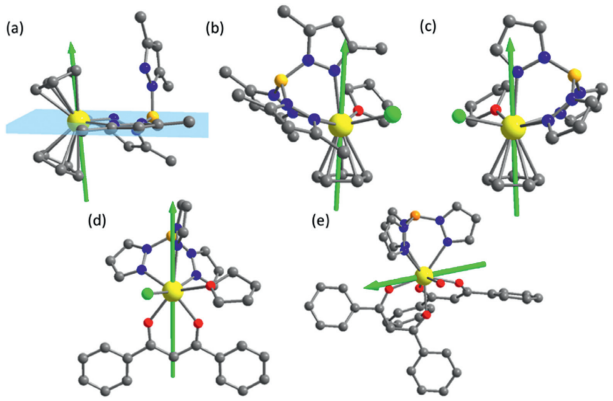

Fig. 4. (a–e) Calculated easy axis of the ground Kramers doublet for **1Dy**–**5Dy**.

cantly affects the dynamic relaxation behaviors, which was further studied using electronic structure calculations. Complete-active-space self-consistent field (CASSCF) calculations using the X-ray determined molecular structures were carried out. The eight lowest spin-orbit energy levels and the corresponding *g* tensors of the complex **1Dy**–**5Dy** were calculated using the SINGLE_ANISO program and listed in Table S3 (Supporting information). The results indicated that the calculated g_z values of Dy^{III} ions in the ground state are close to 20 except those for **1Dy** (18.95) and **5Dy** (19.12). And all of the complexes possess non-negligible transverse components. As shown in Table S3, the g_x and g_y values for **2Dy**, **4Dy** and **5Dy** are larger than those of **1Dy** and **3Dy**. These results are in agreement with magnetic measurements where **2Dy**, **4Dy** and **5Dy** showed faster QTM. The calculated energy gap between the ground and first excited doublets for **1Dy** is 131 K, in good agreement with the experimentally obtained effective energy barrier of 123 K, indicating that the high temperature relaxation is dominated by the Orbach mechanism *via* the first excited state. In contrast, the calculated energy barriers for **2Dy**–**5Dy** are all higher than the experimental energy barriers, possibly due to the influence of the Raman process that reduces the observed energy barrier. For **1Dy**, the two Cp^- anions determine the easy axis of the central Dy^{III} ion, which is close to the normal direction of the N–Dy–N plane (Fig. 4a). The transverse components are caused by the equatorial interactions between Dy^{III} ion and Tp^{*-} anion. When one of the Cp^- was substituted by the Cl^- ion, as demonstrated by **2Dy**, the magnetic easy axis orientates towards the normal direction of the Cp^- ring (Fig. 4b). This indicated that the Cp^- anion provides stronger electrostatic repulsion than the Cl^- and Tp^{*-} anions. Therefore, the Cp^- anion can act as a good axial ligand to stabilize the Ising ground state of the Dy^{III} ion. For **2Dy**, the Cl^-, THF and Tp^{*-} ligands introduce more equatorial interactions, thus contributing to the fast QTM observed. In comparison to **2Dy**, replacing Tp^{*-} by the Tp^- ligand resulted in a smaller Dy–N bond length (2.470(3) Å) along the apical direction of Dy–Cnt(Cp) and a smaller Dy–C bond lengths (2.643(3)-2.689(3) Å) for **3Dy**. The shortened bond lengths will reinforce the interaction along the axial direction of Dy–Cnt(Cp), leading to a larger energy separation between the ground and first excited states. The comparison of **2Dy** and **3Dy** demonstrated that Tp^- ligand can provide a stronger ligand field than Tp^{*-} due to less steric hindrance. When the Tp^- ligand was further substituted by the β-diketonate DBM^- anion, the uniaxial magnetic anisotropy and slow relaxation property of **4Dy** significantly deteriorated. It is attributed to the fact that the DBM ligand cannot provide a strong enough uniaxial ligand field as the Cp^- anion does to stabilize the Ising limit ground state. According to the previous study, the easy axis is largely affected by β-diketonates and usually lies in the plane of diketonates in the Dy^{III}/β-diketonate systems. For **4Dy**, the calculated easy axis is right within the plane of DBM^- and orientates to the N1 atom of Tp^- ligand, in agreement with the paddle-wheel-shaped Dy^{III}/β-diketonate systems. For **5Dy**, the low symmetry and competing interactions between the Tp^- and DBM^- ligands lead to the silence of magnetic relaxation behavior. The comparison of this series of complexes suggests that the strongest electron donor ligand will determine the magnetic main axes and will benefit the high-performance single-molecule magnets (Fig. S13 in Supporting information), whereas the competing interactions between the comparable ligands will diminish the uniaxial anisotropy of the central Dy^{III} ion, thereby weakens the SMMs properties [39,40].

In summary, a series of dysprosium complexes with the combination of cyclopentadienyl, β-diketonate and trispyrazolylborate were synthesized and structurally- and magnetically-characterized. The DC and AC susceptibilities studies revealed that replacing the multidentate ligands can significantly affect the magnetic anisotropy and slow relaxation of magnetization behaviors. The comparison study of them indicated that the cyclopentadienyl anion can provide a stronger uniaxial ligand field than that of β-diketonate and trispyrazolylborate anions. The competitive interactions between the aforementioned ligands lead to the diminishment of the uniaxial anisotropy as well as the observed energy barriers. In addition, complex **3Dy** exhibited a fascinating two-step magnetic relaxation behavior that was caused by the static disordering of the coordinated THF molecule, suggesting that even the second coordination sphere can also have an impact on the electronic structures of the low-lying energy states and thereby the magnetic relaxation behaviors. Thus, to manifest the requirements for the high performance SMMs, the coordination sphere of the central spin carrier should be carefully designed with more concerns on arrangement of strong electron donor ligands and weak electron donor ancillary ligands.

Declaration of competing interest

The authors declare that they have no known competing financial interests or personal relationships that could have appeared to influence the work reported in this paper.

Acknowledgments

This work was financially supported by the National Natural Science Foundation of China (Nos. 22222103, 22173015, 22025101, 21801037, 91961114 and 21871039), and the Fundamental Research Funds for Central University, China. We thank Prof. Bing-Wu Wang from Peking University for the help on *ab initio* calculations and theoretical discussions.

Supplementary materials

Supplementary material associated with this article can be found, in the online version, at doi:10.1016/j.cclet.2022.108055.

References

[1] D.N. Woodruff, R.E.P. Winpenny, R.A. Layfield, Chem. Rev. 113 (2013) 5110–5148.
[2] J.L. Liu, Y.C. Chen, M.L. Tong, Chem. Soc. Rev. 47 (2018) 2431–2453.
[3] F.S. Guo, A.K. Bar, R.A. Layfield, Chem. Rev. 119 (2019) 8479–8505.
[4] Z. Zhu, M. Guo, X.L. Li, et al., Coord. Chem. Rev. 378 (2019) 350–364.
[5] A. Zabala-Lekuona, J.M. Seco, E. Colacio, Coord. Chem. Rev. 441 (2021) 213984.
[6] M.N. Leuenberger, D. Loss, Nature 410 (2001) 789–793.
[7] S. Takahashi, I. Tupitsyn, J. Van Tol, et al., Nature 476 (2011) 76–79.
[8] F. Donati, S. Rusponi, S. Stepanow, et al., Science 352 (2016) 318–321.
[9] J. Long, M.S. Ivanov, V.A. Khomchenko, et al., Science 367 (2020) 671–676.
[10] N. Ishikawa, M. Sugita, T. Ishikawa, et al., J. Phys. Chem. B 108 (2004) 11265–11271.
[11] J.M. Frost, K.L.M. Harriman, M. Murugesu, Chem. Sci. 7 (2016) 2470–2491.

[12] S.G. McAdams, A.M. Ariciu, A.K. Kostopoulos, et al., Coord. Chem. Rev. 346 (2017) 216–239.
[13] A. Dey, P. Kalita, V. Chandrasekhar, ACS Omega 3 (2018) 9462–9475.
[14] M. Feng, M.L. Tong, Chem. Eur. J. 24 (2018) 7574–7594.
[15] S. Sakaue, A. Fuyuhiro, T. Fukuda, et al., Chem. Commun. 48 (2012) 5337–5339.
[16] J.M. Van Raden, D.I. Alexandropoulos, M. Slota, et al., J. Am. Chem. Soc. 144 (2022) 8693–8706.
[17] M.A. AlDamen, J.M. Clemente-Juan, E. Coronado, et al., J. Am. Chem. Soc. 130 (2008) 8874–8875.
[18] Y. Huo, Y.C. Chen, S.G. Wu, et al., Inorg. Chem. 57 (2018) 6773–6777.
[19] Y.S. Meng, S.D. Jiang, B.W. Wang, et al., Acc. Chem. Res. 49 (2016) 2381–2389.
[20] B.M. Day, F.S. Guo, R.A. Layfield, Acc. Chem. Res. 51 (2018) 1880–1889.
[21] X. Yi, K. Bernot, F. Pointillart, et al., Chem. Eur. J. 18 (2012) 11379–11387.
[22] W.M. Wang, S.Y. Wang, H.X. Zhang, et al., Inorg. Chem. Front. 3 (2016) 133–141.
[23] W.Y. Zhang, Y.Q. Zhang, S.D. Jiang, et al., Inorg. Chem. Front. 5 (2018) 1575–1586.
[24] D.I. Alexandropoulos, K.R. Vignesh, H. Xie, et al., Dalton Trans. 48 (2019) 10610–10618.
[25] E.A. Mikhalyova, M. Zeller, J.P. Jasinski, et al., Dalton Trans. 49 (2020) 7774–7789.
[26] J. Long, I.V. Basalov, N.V. Forosenko, et al., Chem. Eur. J. 25 (2019) 474–478.
[27] S. Yu, Z. Hu, Z. Chen, et al., Inorg. Chem. 58 (2019) 1191–1200.
[28] J. Liu, Y.C. Chen, J.L. Liu, et al., J. Am. Chem. Soc. 138 (2016) 5441–5450.
[29] F.-S. Guo, B.M. Day, Y.C. Chen, et al., Science 362 (2018) 1400–1403.
[30] D. Gatteschi, R. Sessoli, J. Villain, Molecular Nanomagnets, Oxford University Press, Demand, 2006.
[31] A. Lunghi, F. Totti, S. Sanvito, et al., Chem. Sci. 8 (2017) 6051–6059.
[32] D.H. Moseley, S.E. Stavretis, Z. Zhu, et al., Inorg. Chem. 59 (2020) 5218–5230.
[33] Y. Ma, Y.Q. Zhai, Q.C. Luo, et al., Angew. Chem. Int. Ed. 61 (2022) e202206022.
[34] G.H. Dieke, H. Crosswhite, Appl. Opt. 2 (1963) 675–686.
[35] K.S. Cole, R.H. Cole, J. Chem. Phys. 9 (1941) 314–351.
[36] J. Soeteman, L. Bevaart, A.J. Van Duyneveldt, Physica 74 (1974) 126–134.
[37] S.D. Jiang, B.W. Wang, H.L. Sun, et al., J. Am. Chem. Soc. 133 (2011) 4730–4733.
[38] W.-B. Sun, B. Yan, Y.Q. Zhang, et al., Inorg. Chem. Front. 1 (2014) 503–509.
[39] X.L. Li, L. Zhao, J. Wu, et al., Chem. Sci. 13 (2022) 10048–10056.
[40] M. Wang, Y. Guo, Z. Han, et al., Inorg. Chem. 61 (2022) 9785–9791.